Front. Phys., 2011, 6(3): 313–319
DOI 10.1007/s11467-011-0162-7

RESEARCH ARTICLE

Theoretical study of photon emission from single quantum dot emitter coupled to surface plasmons

Guang-cun SHAN (单光存)[1,2], **Shu-ying BAO** (包术颖)[3,†], **Kang ZHANG** (张康)[4], **Wei HUANG** (黄维)[1]

[1] *Institute of Advanced Materials (IAM), Nanjing University of Posts and Telecommunications, Nanjing 210003, China*
[2] *Department of Physics and Materials Science, City University of Hong Kong, Kowloon, Hong Kong, China*
[3] *Department of Physics, Fudan University, Shanghai 200433, China*
[4] *School of Information and Electronics, Beijing Institute of Technology, Beijing 100081, China*
E-mail: [†] *bao.shuying@gmail.com*

Received November 15, 2010; accepted December 14, 2010

Motivated by the recent pioneering advances on nanoscale plasmonics and also nanophotonics technology based on the surface plasmons (SPs), in this work, we give a master equation model in the Lindblad form and investigate the quantum optical properties of single quantum dot (QD) emitter coupled to the SPs of a metallic nanowire. Our main results demonstrate the QD luminescence results of photon emission show three distinctive regimes depending on the distance between QD and metallic nanowire, which elucidates a crossover passing from being metallic dissipative for much smaller emitter–nanowire distances to surface plasmon (SP) emission for larger separations at the vicinity of plasmonic metallic nanowire. Besides, our results also indicate that, for both the resonant case and the detuning case, through measuring QD emitter luminescence spectra and second-order correlation functions, the information about the QD emitter coupling to the SPs of the dissipative metallic nanowire can be extracted. This theoretical study will serve as an introduction to understanding the nanoplasmonic imaging spectroscopy and pave a new way to realize the quantum information devices.

Keywords quantum plasmonics, quantum optics, metallic nanowire, surface plasmon (SP), quantum dot

PACS numbers 32.80.Qk, 42.50.-p, 73.20.Mf, 73.21.-b, 73.43.Lp

1 Introduction

In recent years, there have been rapid developments in the fields of nanoscale plasmonics and nano-optics technology based on the surface plasmon (SP) for various applications [1–7]. SPs associated with subwavelength metallic systems are bound, nonradiative electromagnetic excitations associated with charge density waves along the surface of a conducting nanostructure [7]. The unique properties of SPs on conducting nanostructures have produced a number of substantial applications, such as single-molecule detection with surface-enhanced Raman scattering (SERS) [1–4], subwavelength imaging [5], and plasmonic resonance energy transfer (PRET)-based molecular imaging technique [6]. In 2004, Xu *et al.* have presented a master equation model study of surface-enhanced resonant Raman scattering and fluorescence focusing on the interplay between electromagnetic effects and the molecular dynamics, and further examined whether single molecule sensitivity in SERS can be explained in the framework of classical electromagnetic theory [4]. The small transverse-mode area also enables one to strongly couple an emitter to the plasmon, giving rise to a substantial Purcell effect with a Purcell factor of 10^2 or larger. Surface plasmon polaritons (SPPs) play a key role in breaking down the diffraction limit of conventional optics because they allow the compact storage of optical energy in electron oscillations at the interfaces of metals and dielectrics. In particular, an experimental demonstration of nanoscale plasmonic lasers has been realized, and direct measurements

of the emission lifetime reveal a broadband enhancement of the nanostructure's exciton spontaneous emission rate by up to six times, owing to the strong mode confinement and the signature of apparently threshold-less lasing [7]. On one hand, from the point of view of single-molecule spectroscopy (SMS) technique, the single-molecule (SM) spectra are extremely sensitive to the local nanoenvironment in which the SM is situated, so that the fluorescence spectra of the SM will fluctuate in time due to changes in the local environment [8]. The fluorescence photon emission is collected through the transmissive substrate with a high numerical aperture microscope objective; meanwhile, the far-field images are generally taken with the same microscope with the fiber tip removed. In near-field imaging of SMS, a cylindrical aluminum-coated optical fiber tip is used as the excitation source [1, 2], and the excitation is focused by the objective lens. As a result, in a near-field microscope, the metal coating could probably perturb the optical measurements of fluorescence observables of single nanostructure of interest. On the other hand, from the viewpoint of quantum information science and technology, generating strong, coherent interactions between individual quantum emitters and photons is one of the key ingredients for photon-based quantum information processing [9]. Usually, the cavity-mediated coupling between quantum emitters and photons are employed for quantum information processing [10]. In 2006, a method that enables strong, coherent coupling between individual atomic emitters and electromagnetic excitations in conducting nanowires at optical frequencies, via excitation of guided plasmons localized to nanoscale dimensions, was proposed [11]. Moreover, because of the nanowire cylindrical geometry and thus its simple analytical solution, several theoretical studies on atomic qubit–nanowire system have considered the full quantum behavior of plasmon modes with the goal of making devices for quantum information processing [11–16].

Motivated by these recent pioneering advances, in this work, we investigate the quantum optical properties of single quantum dot (QD) emitter coupled to the quantum plasmons of a metallic nanowire. This paper is organized as follows. In Section 2, we firstly give the master equation model of single QD emitter coupled to the SP of metallic nanowire surrounded by some positive dielectric medium, and then present the theory and calculation of electromagnetic modes and also the decay rate due to near-field interaction of dipole of QD with metallic nanowires. We calculate the dissipation rate of the fundamental mode as it propagates along the nanowire due to metallic losses. In Section 3, we calculate the photon emission properties of a QD emitter at the vicinity of plasmonic metallic nanowire as a function of emitter-nanowire distances. Finally, in Section 4, we summarize our results and discuss some future prospects in this new area.

2 Model

In this section, we firstly give the master equation model of single QD emitter coupled to the SP of metallic nanowire surrounded by some positive dielectric medium (Fig. 1), and then present the theory and calculation of electromagnetic modes and also the decay rate due to near-field interaction of dipole of QD with nanoplasmonic metallic nanowires.

Fig. 1 Schematic illustration of the QD–nanowire system: a QD emitter (*red dot*), is placed at a distance d of a metallic nanowire (*blue cylindrical wire*) with radius R.

2.1 Master equation in the markov approximation

In order to understand the fundamental effect of quantum optics properties of QD emitter due to the strong coupling of SP reservoir of metallic nanowire, we concentrate on studying the photon statistics of the light emitted by the single QD emitter in the context of the usual Markovian case of having a resolution in time larger than a picosecond. Strong emitter-SP coupling could be expected when the emitter-nanowire distance is small compared with the wavelength of the emitted light. The strong coupling is possible due to the small mode volume associated with this subwavelength confinement. Therefore, the system coherently driven by a laser can be described by a Markovian dynamics governed by a master equation in the general Lindblad form such as [17, 18]

$$\frac{\mathrm{d}}{\mathrm{d}t}\rho = L\rho = \frac{1}{\mathrm{i}\hbar}[H,\rho] + L_{\mathrm{diss}}\rho \tag{1}$$

where, ρ is the density matrix for the QD–plasmon system, H is the Hamiltonian for the QD–plasmon system, and L_{diss} is the dissipation terms account for various processes. The dissipations lead to nonunitary evolution given by [8, 17, 18]

$$L_{\mathrm{diss}} = \frac{\gamma(t)}{2}\left[2\sigma^{-}\rho(t)\sigma^{+} - \sigma^{+}\sigma^{-}\rho(t) - \rho(t)\sigma^{+}\sigma^{-}\right] \tag{2}$$

where γ is the decay rate. It is worth noting that the influence of metallic nanowire on the decay rate of a single emitter is interesting from both a theoretical and a practical point of view. The small mode volume associated with the fundamental plasmon mode of a nanowire offers a possible mechanism to achieve strong coupling

with nearby optical quantum emitters, in analogy to the methods of Refs. [11, 13–16]. The decay rate in the Markovian regime coincides with the long-time limit of $\gamma(t)$, $\gamma(t) = \gamma(t \to \infty)$, allowing to identify γ as simply the spectral function at the frequency of quantum emitter [14, 15]. In our system of interest, the dipole can possibly lose power radiatively to propagating photon modes through excitation of the guided plasmon modes or through nonradiative loss (heating) in the wire. Furthermore, it has been demonstrated that, under certain circumstances, the small mode volume leads to strongly preferential spontaneous emission into the guided plasmon modes via a mechanism equivalent to the Purcell effect in cavity QED [14–18]. The spontaneous emission rate of a dipole emitter, in general, becomes altered from its free-space value in the presence of some dielectric body. It is well known that spontaneous emission rates can be obtained via classical calculations of the fields due to an oscillating dipole near the dielectric body [19]. This calculation closely follows that of Refs. [19, 20] but is briefly presented here for completeness.

2.2 Theory of electromagnetic models and decay rate

Here, without loss of generality, we are particularly interested in the case of a conducting nanowire surrounded by some lossless positive dielectric (Re $\varepsilon_2 < 0, \varepsilon_1 > 0$). Furthermore, a silver nanowire is taken as an example and the electric permittivity of the silver nanowire at this frequency is assumed to correspond to its measured value in thin films, $\varepsilon_2 = -50 + 0.6\mathrm{i}$ [21]. The details of calculating the electromagnetic modes of a nanowire is given in Refs. [15, 20]. For a cylindrical nanowire of radius R of dimensionless electric permittivity ε_2, which is centered along the z axis and surrounded by a second dielectric medium ε_1, one can use separation of variables and find the electric field and magnetic field solutions $\boldsymbol{E}$, $\boldsymbol{H}$ to Maxwell's equations in each dielectric region in terms of cylindrical coordinates [22]. In cylindrical coordinates, the electric field is given by $\boldsymbol{E}_i(\boldsymbol{r}) = \xi_{i,m} E_{i,m}(k_{i\perp}\rho)\mathrm{e}^{\mathrm{i}m\phi}\mathrm{e}^{\mathrm{i}k_{/\!/}z}$, where $i = 1, 2$ denote the regions outside and inside the cylinder, respectively. Here, $k_{/\!/}$ is the longitudinal component of the wave vector, which is related to the vacuum wave vector $k_0 = \omega/c$, electric permittivity ε_i, and transverse wave vector $k_{i\perp}$ by $\varepsilon_i k_0^2 = k_{/\!/}^2 + k_{i\perp}^2$, and m is an integer characterizing the winding of the mode. The functions $\boldsymbol{E}_{i,m}$ represent some normalized mode profiles. A similar expression holds for the magnetic field $\boldsymbol{H}$. $k_i = \sqrt{\varepsilon_i}k_0$ is the wave vector in medium i. The coefficients $E_{i,m}$ and $H_{i,m}$ multiplying the fields are not arbitrary but, instead, must satisfy a set of equations that enforces the necessary boundary conditions at the dielectric interface $\rho = R$. The existence of a nontrivial solution requires that the matrix corresponding to this linear system have zero determinant (det $\boldsymbol{M} = 0$), which upon simplifying yields the mode equation [22]:

$$\begin{aligned}&\frac{m^2 k_{/\!/}^2}{R^2}\left(\frac{1}{k_{2\perp}^2} - \frac{1}{k_{1\perp}^2}\right)^2 \\ &\quad = \left[\frac{1}{k_{2\perp}}\frac{J_m'(k_{2\perp}R)}{J_m(k_{2\perp}R)} - \frac{1}{k_{1\perp}}\frac{H_m'(k_{1\perp}R)}{H_m(k_{1\perp}R)}\right] \\ &\qquad \cdot \left[\frac{k_2^2}{k_{2\perp}}\frac{J_m'(k_{2\perp}R)}{J_m(k_{2\perp}R)} - \frac{k_1^2}{k_{1\perp}}\frac{H_m'(k_{1\perp}R)}{H_m(k_{1\perp}R)}\right]\end{aligned} \tag{3}$$

The above equation, for example, determines the allowed values of $k_{/\!/}$ as functions of m, R, and ε_i. For a conducting nanowire (Re $\varepsilon_2 < 0$), there exists one fundamental TM modes [22] with axial symmetry ($m = 0$), while all higher-order modes are cut off. For this mode, $k_{/\!/}$, $k_{i\perp} \approx C/R$, indicating that the phase velocity is greatly reduced, while the transverse mode area $\mathrm{A_{eff}} \propto R^2$ is localized to a region on the order of the wire size.

Next, we consider a classical oscillating dipole $\boldsymbol{p}_0\mathrm{e}^{-\mathrm{i}\omega t}$ near the nanowire positioned a distance d and calculate the total fields of the system and the emission properties. Taking $\hat{z}$ to be along the axis of the wire, we note that the fundamental SP mode will not couple to a dipole moment $\boldsymbol{p}_0 \propto \hat{\phi}$ oriented along the azimuthal axis due to the azimuthal symmetry of this mode. In the following calculations, we consider a dipole oriented along the radial direction ($\boldsymbol{p}_0 \propto \hat{\rho}$) while noting that the calculation for an orientation along $\hat{z}$ yields qualitatively similar results. For subwavelength nanostructures, by considering the fields in the quasistatic limit ($\boldsymbol{H} \approx 0$), a simplification of electromagnetic field equation is [20]

$$\nabla \cdot \boldsymbol{D} = \rho_{\mathrm{ext}} \tag{4}$$

$$\nabla \times \mathbf{E} = 0 \tag{5}$$

Here, $\rho_{\mathrm{ext}}(\boldsymbol{r})$ is the external charge density, and $\boldsymbol{D}$ is the electric displacement vector. In the quasistatic limit, we essentially assume that we are considering length scales r over which the phases $k_i r$ associated with the electrodynamic Green's function $G_i(\boldsymbol{r}) \propto \mathrm{e}^{-\mathrm{i}k_i r}/r$ are negligible, so that this function can be approximated by the electrostatic version, $G_i(\boldsymbol{r}) \propto 1/r$. Given an external dipole point charge source located at position $\boldsymbol{r}'$ outside the nanowire (with radial coordinate $\rho' = d$), so that

$$\rho_{\mathrm{ext}}(\boldsymbol{r}, \boldsymbol{r}') = (\boldsymbol{p_0} \cdot \nabla')\,\delta(\boldsymbol{r} - \boldsymbol{r}') \tag{6}$$

To solve for the fields, it is convenient to further separate Φ_1 into "free" and "reflected" components Φ_0 and Φ_r, respectively, where Φ_r represents a source-free contribution that ensures that boundary conditions are satisfied and Φ_0 is the solution for a point charge in a medium of uniform electric permittivity ε_1. Then, one can expand the known source term Φ_0 in an appropriate basis for the cylindrical geometry and expand the source-free terms $\Phi_{r,2}$ in a similar basis that satisfies Laplace's equation $\left(\nabla^2 \Phi_{r,2} = 0\right)$. The unknown coefficients multiplying the basis functions of $\Phi_{r,2}$ will then be determined by im-

posing the proper boundary conditions at the dielectric interface. These expansions are given by [22]

$$\Phi_0(\boldsymbol{r},\boldsymbol{r}') = \frac{1}{4\pi\varepsilon_0\varepsilon_1}\frac{1}{|\boldsymbol{r}-\boldsymbol{r}'|} = \frac{1}{2\pi^2\varepsilon_0\varepsilon_1}\sum_{m=0}^{\infty}(2-\delta_{m,0})\cos[m(\phi-\phi')] \cdot \int_0^{\infty} \mathrm{d}h \cos[h(z-z')] K_m(h\rho') I_m(h\rho), \quad \rho<\rho' \tag{7}$$

$$\Phi_r(\boldsymbol{r},\boldsymbol{r}') = \frac{1}{2\pi^2\varepsilon_0}\sum_{m=0}^{\infty}(2-\delta_{m,0})\cos[m(\phi-\phi')] \cdot \int_0^{\infty} \mathrm{d}h\alpha_m(h)\cos[h(z-z')] K_m(h\rho') K_m(h\rho) \tag{8}$$

$$\Phi_2(\boldsymbol{r},\boldsymbol{r}') = \frac{1}{2\pi^2\varepsilon_0}\sum_{m=0}^{\infty}(2-\delta_{m,0})\cos[m(\phi-\phi')] \cdot \int_0^{\infty} \mathrm{d}h\beta_m(h)\cos[h(z-z')] K_m(h\rho') I_m(h\rho) \tag{9}$$

where $\alpha_m(h)$ and $\beta_m(h)$ thus far are unknown amplitude coefficients. We obtain a set of two coupled equations for $\alpha_m(h)$ and $\beta_m(h)$ by requiring continuity of Φ and $\boldsymbol{D}_\perp$ at the boundary, $\rho = R$. Because of the translational symmetry of the system, these equations are uncoupled in h and can easily be solved. The solutions are given by [22]

$$\alpha_m(h) = \frac{1}{\varepsilon_1}\frac{(\varepsilon_2-\varepsilon_1) I_m(hR) I'_m(hR)}{\varepsilon_1 I_m(hR) K'_m(hR) - \varepsilon_2 K_m(hR) I'_m(hR)} \tag{10}$$

$$\beta_m(h) = \frac{I_m(hR) K'_m(hR) - K_m(hR) I'_m(hR)}{\varepsilon_1 I_m(hR) K'_m(hR) - \varepsilon_2 K_m(hR) I'_m(hR)} \tag{11}$$

To calculate the radiative emission into free space, we consider the far-field properties of the system. Physically, the presence of the emitter induces some dipole moment $\delta\boldsymbol{p}$ in the nanowire, which results in a total radiated power proportional to the square of the total dipole moment of the system, $P_{\mathrm{rad}} \propto \Gamma_{\mathrm{rad}} \propto |\boldsymbol{p}_0 + \delta\boldsymbol{p}|^2$. It is straightforward to obtain that the $m = 1$ term in Eq. (8) is responsible for this contribution, with all other m terms yielding faster decays in ρ. The integral can be given exactly as

$$\Phi_r^{(m=1)}(\boldsymbol{r},\boldsymbol{r}') \approx -\frac{1}{4\pi\varepsilon_0\varepsilon_1}\frac{\varepsilon_2-\varepsilon_1}{\varepsilon_2+\varepsilon_1}\cos(\phi-\phi') \cdot \frac{R^2}{\rho'}\frac{\rho}{\left[\rho^2+(z-z')^2\right]^{3/2}} \tag{12}$$

with a corresponding reflected potential

$$\Phi_{\mathrm{dipole},r}^{(m=1)}(\boldsymbol{r},\boldsymbol{r}') = (\boldsymbol{p}_0\cdot\nabla')\,\Phi_r^{(m=1)}(\boldsymbol{r},\boldsymbol{r}') \approx -\frac{p_0}{4\pi\varepsilon_0\varepsilon_1}\frac{\varepsilon_2-\varepsilon_1}{\varepsilon_2+\varepsilon_1}\cos(\phi-\phi') \cdot \frac{R^2}{d^2}\frac{\rho}{\left[\rho^2+(z-z')^2\right]^{3/2}} \tag{13}$$

for the choice of parameters $\rho' = d$, $z' = 0$, and $\boldsymbol{p}_0 = p_0\hat{\rho}$. By comparing Eq. (13) to the potential due to a dipole $\delta\boldsymbol{p}$ in uniform dielectric ε_1, $V_{\delta\boldsymbol{p}} = \frac{\delta\boldsymbol{p}\cdot\boldsymbol{r}}{4\pi\varepsilon_0\varepsilon_1 r^3}$ [11], we can readily have

$$\delta\boldsymbol{p} = p_0\frac{\varepsilon_2-\varepsilon_1}{\varepsilon_2+\varepsilon_1}\frac{R^2}{(R+d)^2}\hat{\rho} \tag{14}$$

Finally, the radiative spontaneous emission rate for a QD emitter near the nanowire is given by [20]

$$\frac{\gamma_r}{\gamma_0} = \left|1+\frac{\varepsilon_2-\varepsilon_1}{\varepsilon_2+\varepsilon_1}\frac{R^2}{(R+d)^2}\right|^2 \tag{15}$$

Here, $\gamma_0 = \omega_0^3 p^2/(3\pi\varepsilon_0 c^3)$, which is the spontaneous emission rate of the QD emitter in uniform dielectric free space. Away from the plasmonic resonance, the radiative decay rate changes slightly from γ_0 due to a small change in the radiative density of states in the vicinity of the nanowire. In Fig. 2, the decay rate versus emitter–nanowire separation distance is plotted, in units of the QD emitter spontaneous decay rate in free space γ_0.

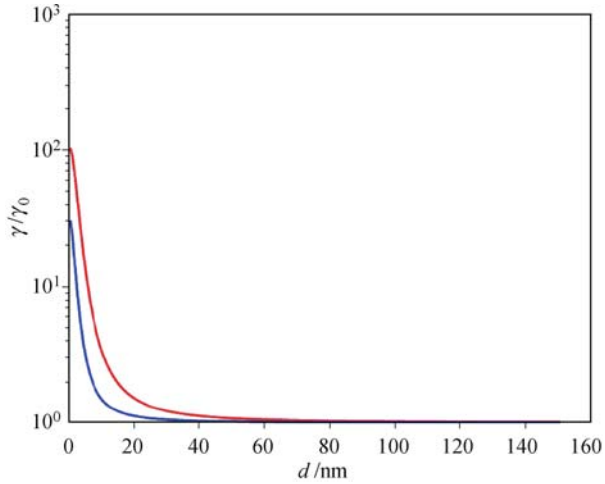

Fig. 2 Calculated relative decay rate γ/γ_0 as a function of QD–nanowire distance d. Blue curve for $R = 5$ nm; Red curve for $R = 10$ nm.

2.3 Master equation in the rotating frame

Assuming a simple nondegenerate atomic two-state QD in an external classical laser field, hereafter, the density-matrix master equation of the QD–plasmon system coherently driven by a laser with the laser frequency, ω_L in the rotating frame, is given by [16–18]

$$\frac{\mathrm{d}\rho(t)}{\mathrm{d}t} = \mathrm{i}\left\{\Delta\omega\left[\rho(t),\sigma^+\sigma^-\right] + \frac{\Omega}{2}\left[\rho(t),\sigma^+ + \sigma^-\right]\right\} + \frac{\gamma}{2}\left[2\sigma^-\rho(t)\sigma^+ - \sigma^+\sigma^-\rho(t) - \rho(t)\sigma^+\sigma^-\right] \tag{16}$$

where $\Delta\omega = \omega_0 - \omega_L$, and Ω is the Rabi frequency measuring the strength of the coupling of the QD emitter dipole with the laser field. Hereafter, we use the units of the spontaneous decay rate of the QD emitter in free space γ_0, and focus on the resonance fluorescence of QD emitter near the dissipative surface of a metallic nanowire to extract the fundamental effect of quantum optics properties of QD emitter due to the strong coupling of SP reservoir of metallic nanowire.

3 Results and discussion

The enhanced decay rate of single QD emitter due to the SP reservoir of the nanowire surface is depicted in Fig. 2. As indicated in Fig. 2, when the emitter-nanowire distance varies, the decay rate undergoes a transition. Under certain circumstances, emission into the guided plasmon modes is greatly enhanced over decay into radiative and nonradiative channels. At very short distances, the decay rate is highly enhanced with respect to spontaneous decay rate in free space and shows a $1/d^3$ dependence, which can be obtained by means of a model that only contains nonradiative processes as the creation of electron-hole pairs in the metallic medium. For larger separations beyond a critical distance, the QD decay just produces the photon emission and approaches a stable value. It should be pointed out that, in the case of the single QD embedded in a dielectric or a metal with very large losses, this crossover can be hindered by other physical effects, such as those coming from local dissipative circulating currents [19].

In order to calculate the correlation function and fluorescence spectra numerically, from the master Eq. (16), one can derive the equations of motion for the expectation values. For such a case of a simple nondegenerate atomic two-state QD emitter in a coherent classical laser field, the QD emitter can be described by 2×2 density matrix ρ whose elements are ρ_{ee}, ρ_{gg}, ρ_{eg}, and ρ_{ge}. Using Eq. (16), the stochastic optical Bloch equations, in the rotating wave approximation, are [18, 23]

$$\dot{\rho}_{gg} = \gamma\rho_{ee} + \mathrm{i}\frac{1}{2}\Omega\left(\rho_{eg} - \rho_{ge}\right)\mathrm{e}^{-\mathrm{i}\omega_L t} \tag{17-1}$$

$$\dot{\rho}_{ge} = -\mathrm{i}\Delta\omega\rho_{ge} - \gamma\rho_{ge} - \mathrm{i}\frac{1}{2}\Omega\left(\rho_{gg} - \rho_{ee}\right)\mathrm{e}^{-\mathrm{i}\omega_L t} \tag{17-2}$$

$$\dot{\rho}_{ee} = -\gamma\rho_{ee} + \mathrm{i}\frac{1}{2}\Omega\left(\rho_{ge} - \rho_{eg}\right)\mathrm{e}^{-\mathrm{i}\omega_L t} \tag{17-3}$$

The steady-state solution for the excited state population is

$$\langle\rho_{ee}\rangle_{ss} = \frac{\Omega^2}{\gamma^2 + 4\Delta\omega^2 + 2\Omega^2} \tag{18}$$

In the resonant case ($\Delta\omega = 0$), we can obtain an analytical solution,

$$\rho_{ee}(t) = \frac{\Omega^2}{\gamma + 2\Omega^2}\left\{1 - \mathrm{e}^{-3\gamma t/4}\left[\cos(Rt) + \frac{3\gamma}{4R}\sin(Rt)\right]\right\} \tag{19}$$

where $R = \sqrt{\Omega^2 - \left(\frac{\gamma}{4}\right)^2}$ is the so-called Rabi splitting at resonance characterizing the strength of the effective coupling. Note that the strongly QD–SP coupling at the single-photon level leads to pronounced modification of photon statistics that cannot be captured by only considering average intensities, but appear in higher-order correlations of the transmitted and reflected fields. Specifically, the normalized second-order correlation function of interest is given by [12, 17]

$$g^{(2)}(t) = \frac{\langle\sigma^{(+)}(t)\sigma^{(+)}(t+\tau)\sigma^{(-)}(t+\tau)\sigma^{(-)}(t)\rangle}{\langle\sigma^{(+)}(0)\sigma^{(-)}(\tau)\rangle\langle\sigma^{(+)}(t)\sigma^{(-)}(t+\tau)\rangle} \tag{20}$$

In the resonant case ($\Delta\omega = 0$), the second-order correlation function can be analytically expressed as [12, 17]

$$g^{(2)}(t) = 1 - \mathrm{e}^{-3\gamma t/4}\left[\cos(Rt) + \frac{3\gamma}{4R}\sin(Rt)\right] \tag{21}$$

Figure 3(a) shows $g^{(2)}(t)$ for zero detuning for three distinctive regimes. As depicted in Fig. 3(a), it clearly exhibits photon antibunching: $g^{(2)}(0)$=0 due to the fact that the emitter can only absorb and re-emit one photon at a time, which has also been demonstratedd by Lukin and his coworkers [12] and also by us using kinetic Monte–Carlo simulation [23]. Apart from the antibunching, $g^{(2)}(t)$ (the blue curve) shows a remarkable oscillatory behavior, and such oscillatory behavior in strong-coupling regime (SCR) with lower-power of laser is observed before the steady-state is achieved, which eventually reflects action of an efficient single-photon switch [12]. Nevertheless, for weak-coupling regime (WCR) of much larger distance of QD–nanowire separation or even in the absence of metallic nanowire, $g^{(2)}(t)$ (the red curve) approaches unity without oscillation for all times owing to saturation of the QD atomic-like response. Furthermore, using the quantum regression theorem, the resonance fluorescence spectra of QD emitter are plotted for three different decay rates γ due to enhancement of SP of metallic nanowire in Fig. 3(b). As shown in Fig. 3(b), the red Lorentzian curve peaked at the QD qubit frequency of about ω_0 with linewidth $\gamma/2$ corresponds to the WCR case for a much larger separation distance ($d >\sim 40$ nm) of QD–nanowire or even in the absence of metallic nanowire, so only a small peak of the light emitted is observed in the spectrum for the WCR. The blue curve corresponds to the transition region from WCR to SCR, where just one main peak and two satellite peaks start to occur at the laser Rabi frequency on top of the Lorentzian peaked at the qubit frequency. For a SCR situation for a much smaller separation distance

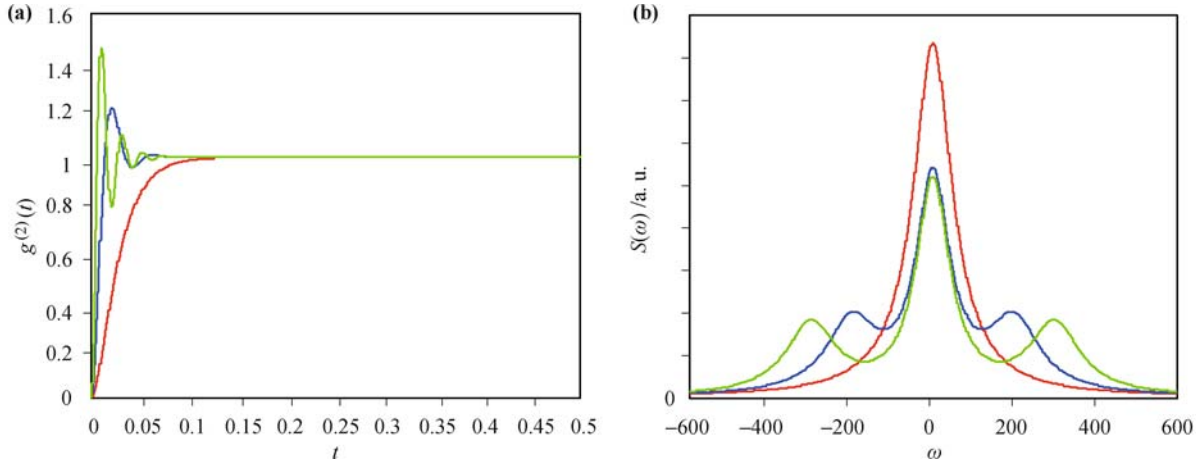

Fig. 3 QD emitter resonance luminescence properties of QD–nanowire system in the resonant laser excitation case for the different separation within the corresponding weak-coupling regime, intermediate regime, and strong-coupling regime, corresponding to values of $\Omega/\gamma = 20\gamma_0/\gamma_0$, $20\gamma_0/4\gamma_0$, and $10\gamma_0/5\gamma_0$ for the red, blue, and green curves, respectively. **(a)** Fluorescence correlation function $g^{(2)}(t)$ for QD–SP system, which indicates the photon antibunching at $t = 0$. **(b)** QD emitter luminescence spectra $S(\omega)$ for three different coupling regimes due to enhancement of SPs of metallic nanowire.

($d \sim 2.5$ nm) of QD–nanowire, these two strong sidebands appear at frequencies $\omega = \omega_0 \pm \Omega$ in the green curve. Notably, we can lower the excitation power of laser to drive the QD weakly. In essential, there are always two main contributions to the resonance fluorescence spectra: the Rayleigh scattering coherent part and the one coming from the incoherent scattering. As a consequence, the QD fluorescence spectra exhibits only one single peaks in absence of plasmonic interaction, whereas the QD fluorescence spectra may exhibit two additional sidebands due to the coupling with plasmonic interaction of metallic nanowire under the same laser coherent excitation conditions. In particular, under resonant excitation, an analytical expression of the fluorescence spectrum is given by

$$S(\omega) \propto \left[\frac{\gamma/4}{\frac{\gamma^2}{4} + (\omega - \omega_0)^2} + \frac{3\gamma/16}{\frac{9\gamma^2}{16} + (\omega - \omega_0 + \Omega)^2} + \frac{3\gamma/16}{\frac{9\gamma^2}{16} + (\omega - \omega_0 - \Omega)^2}\right] \tag{22}$$

Therefore, the luminescence properties are very sensitive to the QD–nanowire separation distance. Our results here are in agreement with the experimental observations about enhancement of SM fluorescence using a gold nanoparticle as an optical nanoantenna [24, 26].

Next, we turn on the detuning case that the laser is out of resonance, the Rabi splitting should be given as

$$R_\Delta = \sqrt{\Omega^2 - \left(\frac{\gamma}{4} + \mathrm{i}\Delta\omega\right)^2} \tag{23}$$

Using the quantum regression theorem, the fluorescence spectra properties are shown in Fig. 4 for three different Ω. As shown in Fig. 4, only one main Lorentzian peak of the red curve corresponds to a case where the QD is strongly coupled to the SPs, and the blue curve occurs peaked at the QD emitter frequency of about ω_0 corresponds to a case for the transition region from WCR to SCR, respectively. For the WCR situation where the QD is weakly coupled to the SPs, two strong sidebands of the green curve appear at laser Rabi frequencies $\omega = \omega_0 \pm \Omega$. In other words, for the non-resonant case, the threshold changes but the behavior remains qualitatively unaffected: even though the dressed state structure is slightly modified by the detuning, a Mollow triplet still exists in the non-resonant case. It is worthwhile noting that the difference between the resonant case and the detuning non-resonant case is that there exist much wider sidebands and linewidth of QD luminescence spectra for the non-resonant case due to the non-resonant excitation interaction of QD with excitation laser. The existence of this Mollow's triplet indicates a manifestation of the strong coupling of the laser to the QD–SP system. In fact, when optimized, the probability of emission into the

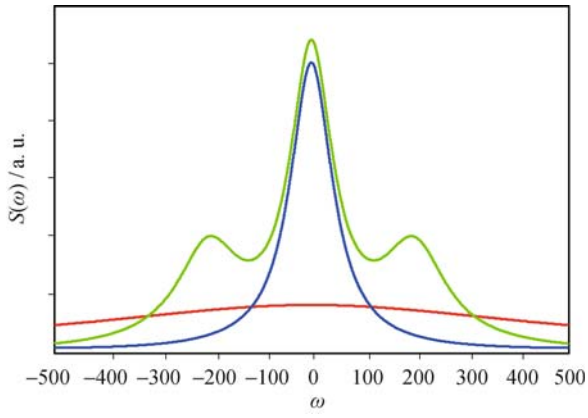

Fig. 4 QD emitter luminescence spectra $S(\omega)$ of QD–nanowire system in the non-resonant laser excitation case for the different separation within the corresponding weak-coupling regime, intermediate regime, and strong-coupling regime, corresponding to values of $\Omega/\gamma = 20\gamma_0/\gamma_0$, $20\gamma_0/4\gamma_0$, and $10\gamma_0/5\gamma_0$ for the red, blue, and green curves, respectively.

plasmon mode approaches almost unity for small R and is limited only by inherent losses in the metal. For both the resonant case and the detuning case, our results indicate that, through measuring QD luminescence spectra and second-order correlation functions, the information about the QD emitter coupling to the SP of the dissipative metallic nanowire can be extracted.

4 Conclusions and perspective

In this work, using a Markov approximation, we have studied the fundamental effect of SP reservoir on photon emission properties of single QD emitter, near the nanowire embedded in the dielectric. The coherent excitation of QD emitter driven by a laser allows the existence of a steady state as well as the analysis of fluorescence spectrum of the QD–SP system, for instance, surface enhancements of decay rate emission, spectra, and photon–photon correlation functions. Our main results demonstrate that the QD luminescence results of photon emission show three distinctive regimes depending on the distance between QD and metallic nanowire, and demonstrate which elucidates a crossover passing from being metallic dissipative for very small emitter-nanowire distances to SP emission for larger separations at nanoscale. Recent advances made in quantum plasmonic have become routine in many laboratories around the world [6, 13–15, 24–26]. Furthermore, it is certain that many of them will require developments of new theoretical concepts as well as plasmonic nanotechnologies. Our next task, beyond the quantum optics scope of the present work, is to treat the plasmonic part of the system not as a reservoir but as an ingredient coherently coupled to one or more QDs and to measure the quantum information entropy using quantum trajectory algorithm. This theoretical study will serve as an introduction to understanding the nanoplasmonic imaging spectroscopy and pave a new way to realize the quantum information devices.

Acknowledgements This work was financially supported by the National Natural Science Foundation of China under Grant No. 60721004, and the National Basic Research Program of China under Grant No. 2009CB010600.

References

1. S. Nie and S. R. Emory, Science, 1997, 275: 1102
2. K. Kneipp, Y. Wang, H. Kneipp, L. T. Perelman, I. Itzkan, R. R. Dasari, and M. S. Feld, Phys. Rev. Lett., 1997, 78: 1667
3. H. X. Xu, J. Aizpurua, M. Käll, and P. Apell, Phys. Rev. E, 2000, 62: 4318
4. H. X. Xu, X. H. Wang, M. Persson, H. Q. Xu, M. Käll, and P. Johansson, Phys. Rev. Lett., 2004, 93: 243002
5. I. I. Smolyaninov, J. Elliott, A. V. Zayats, and C. C. Davis, Phys. Rev. Lett., 2005, 94: 057401
6. G. L. Liu, Y.-T. Long, Y. Choi, T. Kang, and L. P. Lee, Nature Methods, 2007, 4: 1015
7. R. F. Oulton, V. J. Sorger, T. Zentgraf, R.-M. Ma, L. Dai, G. Bartal, and X. Zhang, Nature, 2009, 461: 629
8. G. C. Shan and W. Huang, J. Nanosci. Nanotechnol., 2009, 9: 1176
9. A. K. Ekert, Phys. Rev. Lett., 1991, 67: 661
10. R. J. Thompson, G. Rempe, and H. J. Kimble, Phys. Rev. Lett., 1992, 68: 1132
11. D. E. Chang, A. S. Sørensen, P. R. Hemmer, and M. D. Lukin, Phys. Rev. Lett., 2006, 97: 053002
12. D. E. Chang, A. S. Sørensen, E. A. Demler, and M. D. Lukin, Nat. Phys., 2007, 3: 807
13. L. Childress, A. S. Sørensen, and M. D. Lukin, Phys. Rev. A, 2004, 69: 042302
14. A. V. Akimov, A. Mukherjee, C. L. Yu, D. E. Chang, A. S. Zibrov, P. R. Hemmer, H. Park, and M. D. Lukin, Nature, 2007, 450: 402
15. Y. N. Chen, G. Y. Chen, D. S. Chuu, and T. Brandes, Phys. Rev. A, 2009, 79: 033815
16. D. Dzsotjan, A. S. Sorensen, and M. Fleischhauer, Phys. Rev. B, 2010, 82: 075427
17. M. O. Scully and M. S. Zubairy, Quantum Optics, Cambridge: Cambridge University Press, 1999
18. H. P. Breuer and F. Petruccione, The Theory of Open Quantum Systems, Oxford: Oxford University Press, 2002
19. J. M. Wylie and J. E. Sipe, Phys. Rev. A, 1984, 30: 1185
20. V. V. Klimov and M. Ducloy, Phys. Rev. A, 2004, 69: 013812
21. P. B. Johnson and R. W. Christy, Phys. Rev. B, 1972, 6: 4370
22. J. D. Jackson, Classical Electrodynamics, New York: Wiley, 1999
23. G. C. Shan and W. Huang, Front. Phys. China, 2006, 1(4): 405
24. S. Kühn, U. Håkanson, L. Rogobete, and V. Sandoghdar, Phys. Rev. Lett., 2006, 97: 017402
25. D. E. Chang, A. S. Sørensen, P. R. Hemmer, and M. D. Lukin, Phys. Rev. B, 2007, 76: 035420
26. H. Wei, D. Ratchford, X. Q. Li, H. X. Xu, and C. K. Shih, Nano Lett., 2009, 9: 4168